DYNAMICS OF VIBRATION-ISOLATED PLATFORMS

Vibration isolation systems are the most important part of state-of-the-art vibration control arsenal. The goal of this White Paper is to help users and designers of vibration-isolated platforms understand basic dynamics of such platforms, methods of describing their performance, advantages and disadvantages of possible principal design solutions.

What makes a mechanical structure a vibration isolation system? What are the main components of a properly designed vibration isolation system? How do they interact? What are the general methods of improving the quality of a vibration isolation system? These are the questions we'll address.

Any well-designed vibration isolation system has two main components: soft isolators and a stiff platform. Isolated platforms are the mainstay of vibration control techniques in precision optomechanics and photonics. The prime examples of such platforms are state-of-the-art optical tables with honeycomb cores; other examples include granite slabs, frames, solid plates, stiff casings, and other structures perceived as sturdy and stable. Pneumatic isolators are a "workhorse" of precision vibration control; spring-based and elastomer-based isolators find their applications, too.

The platform, designed to carry vibration-sensitive optomechanical applications, should be as stiff as possible to minimize misalignment of optical paths. Ideally, the platform should behave as an absolutely rigid body; unfortunately, absolutely rigid bodies do not exist. As an elastic plate-like structure, the platform can experience flexural vibrations following the shapes of bending, twisting, and combinations thereof. Sharp deviations from rigid-body behavior may happen in form of structural resonances at the frequencies close to the natural frequencies of the platform. Resonance vibrations of a platform carrying optomechanical equipment can be excited by residual impacts coming from the floor through isolators, by acoustical inputs, by atmospheric turbulence and by on-board sources. They can lead to relative motion and misalignment of parts of the platform, which may affect optical performance.

We'll start from the dynamic model of the contemporary state-of-the-art two-chamber pneumatic isolator and then proceed to the detailed dynamic analysis of the full mechanical model containing isolators supporting a flexible platform. Real-life platforms such as optical tables are three-dimensional structures with rather complicated internal structure[1]. Dynamic modeling of their flexural vibration requires numerical analysis. Instead, in this Technical Note we use, for modeling a platform, a simple, familiar and most useful model of an elastic beam vibrating in the vertical direction (see Fig. 1). Kinematic excitation u_0 in Fig. 1(a) models vibration coming from the floor; force excitation F in Fig. 1(b) models effects of acoustical, atmospheric and on-board sources, as well as standard dynamic compliance (hammer) test.

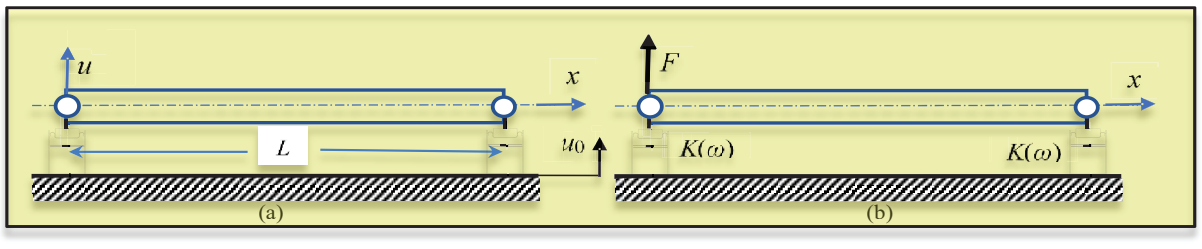

Figure 1. Model of a pneumatically isolated platform. a) kinematic excitation from the floor; (b) force excitation.

[1] https://www.newport.com/n/vibration-control-systems

The advantage of this modeling approach is that all calculations can be made in an explicit analytical form. They can be followed and verified using standard college math. On the other hand, the model has all the features of a real-life isolated platform – rigid body motion with linear and rocking modes, and a sequence of flexural vibration modes. Applying the forces and elastic supports at the ends of the beam greatly simplifies analytical development: we can resolve all cases simply by adding proper boundary conditions to the beam equation.

We shall consider vibration of the foundation (deriving vibration transmissibility) and dynamic force applied at the end of the beam (deriving dynamic compliance), and describe real vs. rigid body behavior including the relative motion of points of the beam and misalignment of different areas of the beam. We'll then study the influence of varying mass and bending stiffness of the platform. Finally, we'll model the damping effect of tuned mass dampers (TMD) by attaching a spring-damper-mass system to each end of the beam.

A. Mechanical Model of the Pneumatic Vibration Isolator

To bring the model closer to reality, we'll employ a realistic model of pneumatic vibration isolator instead of a spring-and-dashpot model considered in earlier Technical Note .

A pneumatic chamber, also known as an acoustic cavity, is the "heart" of a pneumatic vibration isolator. The linear stiffness of the pneumatic chamber is given by the following equation:

$$K_c = \gamma \frac{p_0 A^2}{V}. \qquad (1)$$

Here p_0 is the total pressure, A is the piston area, and V is the internal volume; γ is an adiabatic constant, equal to 1.41 for air. Equation (1) illustrates one of the most valuable properties of a pneumatic isolator, namely, its ability to adjust the stiffness to the load. Since the pressure increases with the supported weight, the natural frequency stays almost constant in a range of supported loads.

Another element of the pneumatic isolator is a diaphragm, sometimes called "rolling diaphragm," that seals the air volume and allows free motion of the piston in process of re-leveling. Equation (1) is still applicable with *A* meaning an effective piston area that covers the space up to half-span of the inflated diaphragm.

Damping is necessary in isolation systems in order to limit the resonance amplification. To this effect, a double chamber "self-damping" design is used in state-of-the-art pneumatic vibration isolators. The air volume is divided into two chambers: the upper one, V_1, called a compliance chamber, and the lower one, V_2, called a damping chamber or a surge chamber. The two chambers are connected by a flow resistance orifice that is designed to provide a laminar viscous flow of gas between the two chambers. The schematics of the resulting device is shown in Fig. 2 (a). This is equivalent to the mechanical model shown in Fig. 2(b). See the paper[2] if you are interested in the detailed derivation.

Figure 2(b) leads to the formula for the dynamic stiffness of the isolator, that is, the ratio of the complex amplitude of harmonic force, P_1, acting on the isolator, to the complex amplitude of displacement, u_1, of the isolator, as function of frequency:

[2] This part is based on the paper: V.M. Ryaboy, Static and dynamic stability of pneumatic vibration isolators and systems of isolators, Journal of Sound and Vibration, 333 (2014) p. 31–51.
[3] https://www.newport.com/n/vibration-control-fundamentals

Here K_1 represents the stiffness of the upper chamber and K_2 represents the stiffness of the lower chamber via Eq. (1); C_{12} represents the viscosity of the gas moving through the orifice.

$$K(\omega) = \frac{1}{\frac{1}{K_1} + \frac{1}{K_2 + i\omega C_{12}}} + K_d. \quad (2)$$

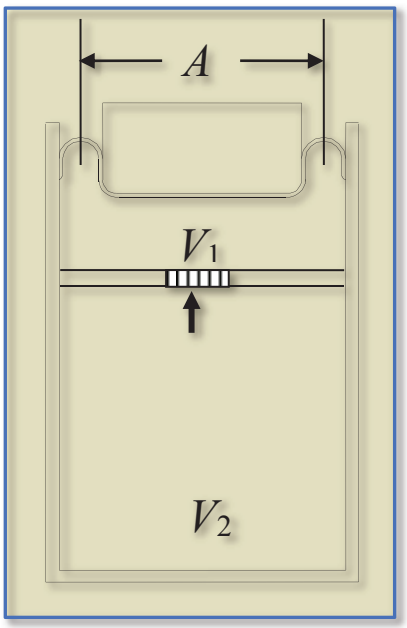

(a)

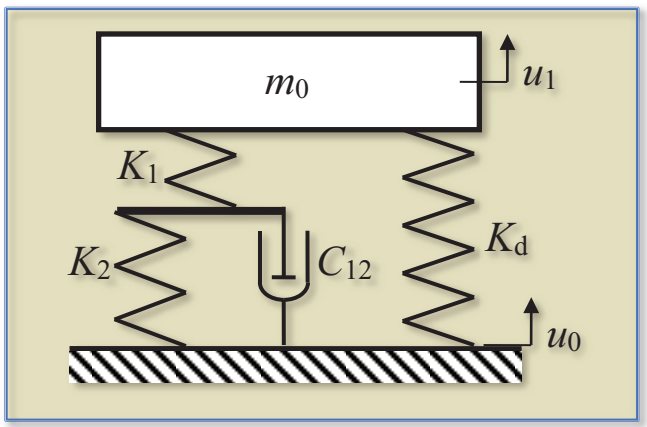

(b)

Figure 2. Schematic representation of a pneumatic vibration isolator (a) and its mechanical model (b).

This is a complex stiffness that describes elastic and dissipative components. From Eq. (2), as well as from the qualitative analysis of Fig. 2(b), follows that the dynamic stiffness has two limiting values: at low frequencies ($\omega \to 0$) the flow resistance of the orifice is low, and K(ω) assumes the lowest value, K_L, which corresponds to both chambers acting as one:

$$K_L = \frac{K_1 K_2}{K_1 + K_2} + K_d = \frac{\gamma p_0 A^2}{V_1 + V_2} + K_d.;$$

Low-frequency (static) stiffness K_L defines the nominal natural frequency of the isolator. In our case

$$f_0 = \frac{\omega_0}{2\pi} = \frac{1}{2\pi}\sqrt{\frac{2K_L}{m}}.$$

Static stiffness of one isolator equals

$$k = K_L = \tfrac{1}{2} m\omega_0^2. \quad (3)$$

At high frequencies, the flow resistance grows, and $K(\omega)$ approaches the highest limiting value, K_H, which corresponds to the top chamber acting alone:

$$K_H = K_1 + K_d = \frac{\gamma p_0 A^2}{V_1} + K_d.$$

Damping can be normalized to the time constant, τ, of the pressure equalizing between the chambers, as follows: $\tau = C_{12}/(K_1+K_2)$. Using these values, the dynamic stiffness can be written in the following compact form:

$$K(\omega) = K_L \frac{1 + R \cdot i\omega\tau}{1 + i\omega\tau}, \quad (4)$$

where R =K_H/K_L. We'll use this expression for the frequency-dependent stiffness in researching the dynamics of vibration isolation platforms in the next sections of this Technical Note. We'll assume f_0 = 1 Hz, R = 16, τ = 0.02 s, which is close to the parameters of the MKS state-of-the-art pneumatic vibration isolator S2000-A.

For detailed analysis of the performance of a standalone pneumatic isolator or a group of isolators supporting an optical table, see paper[2].

B. Isolated Platform: Transmissibility and Dynamic Compliance; Rigid Body Line; Relative Motion and Misalignment

To approach the problem in a systematic manner, let us first study the dynamics of the isolated platform as if it were absolutely rigid: assume the beam in Fig. 1 is a rigid body, and find its motion under kinematic and force excitations. In the first case (Fig. 1 a), we assume that the foundation experiences harmonic vibration $\boldsymbol{u_0}e^{i\omega t}$. Due to symmetry, the rigid beam responds with linear harmonic oscillation $\boldsymbol{u}e^{i\omega t}$. The equation of motion in the frequency domain is

$$-m\omega^2 + 2K(\omega)(u-u_0) = 0. \qquad (5)$$

The complex ratio of amplitudes $\boldsymbol{u/u_0}$ is called the vibration transmissibility. It is a function of frequency ω. According to equations (4) and (5),

$$\frac{u}{u_0} = \frac{1}{1-\dfrac{\omega^2}{\omega_0^2}\dfrac{1+i\omega\tau}{1+R\cdot i\omega\tau}},$$

where $\omega_0 = \sqrt{2K_L/m} = 2\pi f_0$. The absolute value of this function is plotted in Fig. 3. This graph clearly shows the main property of the isolator: its ability to attenuate vibration transmitted from the floor to the platform. The isolation takes place at frequencies higher than, approximately, $1.4f_0$. There is no isolation below that frequency and even a shallow peak at $f = f_0$. The frequency f_0 cannot be made too low because that would make the system too sensitive to small perturbations, and potentially unstable. One Hertz is generally adopted as the lowest practical value for f_0[4] .

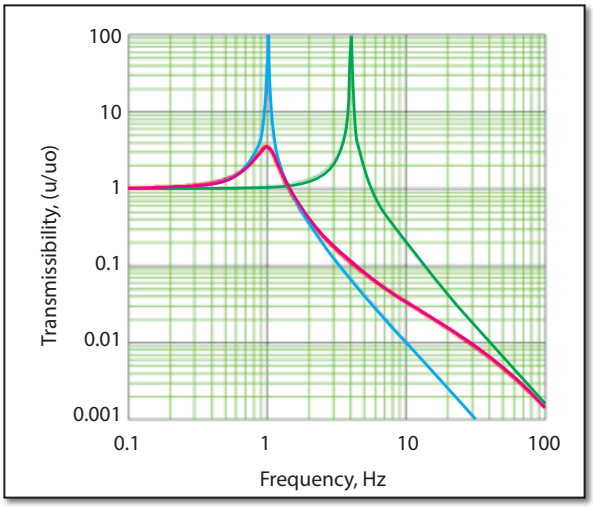

Figure 3. Transmissibility of the pneumatic isolator. Thin lines represent asymptotic behavior at low frequencies when both chambers work as one, and at high frequencies when only the top chamber provides resilience.

In case of force excitation shown in Fig. 1(b) we need to consider both linear and angular motions. A rigid beam has two generalized coordinates (degrees of freedom): vertical displacement of its center of gravity (CG), $\boldsymbol{u_c}$, and rotation around the center of gravity, θ, as shown in Fig. 4, so that

$$u(x) = u_c + \left(x - \frac{L}{2}\right)\theta. \qquad (6)$$

External force ***F*** at the edge can be reduced to the force acting through the CG and rotational moment around CG. As shown in Fig. 5, the edge force of Fig. 1(b) is equivalent to the force F and moment *–FL/2* applied at CG.

(4) A class of more sophisticated vibration isolation systems, called active vibration control systems, such as MKS Guardian® workstation, do not exhibit this resonance and provide isolation at sub-Hertz frequencies, but they are beyond the scope of this Technical Note.

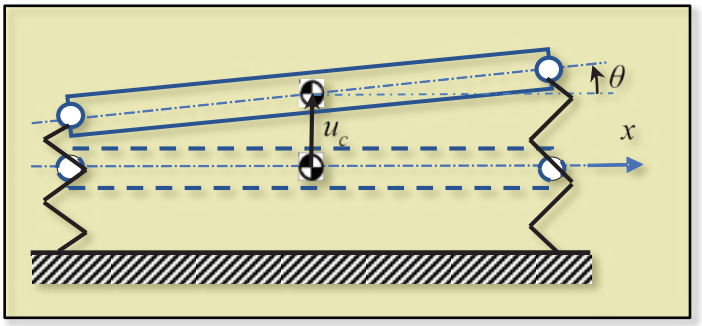

Figure 4. Motion of the beam as a rigid body.

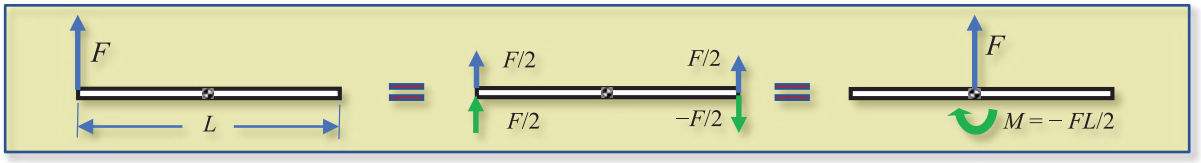

Figure 5. Off-center force on a rigid beam is reduced to force and rotating moment at the center of mass.

The rigid-body motion is composed of linear motion, governed by the equation in the frequency domain for u_c,

$$\left[-m\omega^2 + 2K(\omega)\right]u_c = F \tag{7}$$

and rotational motion, governed by the equation in the frequency domain for θ,

$$\left[-J\omega^2 + K(\omega)\frac{L^2}{2}\right]\theta = -\frac{FL}{2}. \tag{8}$$

For thin beams, the moment of inertia *J* is, approximately,

$$J = \frac{mL^2}{12}. \tag{9}$$

We'll accept this value. To determine the motion of the rigid beam, resolve (7) and (8) for u_c and θ and substitute into (6). Taking into account the expressions for the frequency-dependent stiffness (4), static stiffness (3) and moment of inertia (9), one arrives at the following formula for the transfer function from F to the displacement at any point of the beam:

$$\frac{u(x)}{F} = \frac{1}{k}\left[\frac{1}{2\left(\frac{1+Ri\omega\tau}{1+i\omega\tau} - \frac{\omega^2}{\omega_0^2}\right)} + 3\left(\frac{1}{2} - \frac{x}{L}\right)\frac{1}{3\left(\frac{1+Ri\omega\tau}{1+i\omega\tau}\right) - \frac{\omega^2}{\omega_0^2}}\right]. \tag{10}$$

This function is plotted in Fig. 6 for $x = 0$. Note that the rocking mode of the beam is excited in this case along with the linear vertical motion. To obtain results in non-dimensional form, it is referred to the local static compliance, ***1/k***. The transfer function ***u*(0)/*F*** is called ***dynamic compliance***. It is widely used for illustration of dynamic properties of vibration-isolated platforms. The dashed line in this graph is the ideal rigid body line describing the reaction of free-floating absolutely rigid body. This line is defined by the mass and moment of inertia. Both lines coincide at frequencies sufficiently higher than the resonance frequencies of the isolation system, placed, according to (10), at, approximately, 1 Hz and 1.7 Hz.

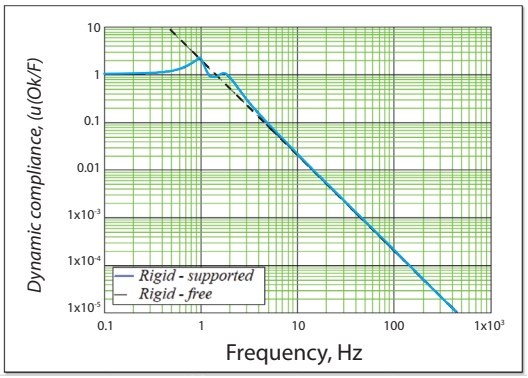

Figure 6. Dynamic compliance described by rigid – body lines for free and supported rigid beams.

Returning to the elastic beam, we must start from the equation of motion. The differential equation for dynamic bending of a beam is derived in many vibration textbooks and handbooks. We'll not repeat the derivation here. For the classical (Bernoulli-Euler) model, based on the assumption that the

cross-sections stay flat and normal to the axis of the beam, the equation is

$$\rho A\ddot{u}(x,t) = -\frac{\partial^2}{\partial x^2}\left(EI\frac{\partial^2 u(x,t)}{\partial x^2}\right) + p(x,t), \tag{11}$$

where ***u*** is the lateral (vertical) displacement, ***E*** is the Young's modulus, I is the moment of inertia of the cross-section, ρ is the mass density, ***A*** is the area of the cross-section, p is the lateral force per unit length; ***x*** is the coordinate along the beam's central axis. We'll assume that A and EI are constant (independent of ***x***).

Constitutive equation for the Bernoulli-Euler beam relates the moment M_c acting on the beam's cross-section to the curvature of the deformed axis of the beam, equal, in the linear approximation, to the second derivative of the displacement:

$$M = EI\frac{\partial^2 u}{\partial x^2}. \tag{12}$$

The shear force in the cross-section is

$$Q = \frac{\partial M}{\partial x}. \tag{13}$$

The sign convention is illustrated in Fig. 7. To study the vibrational properties of the beam, we introduce a complex amplitude ***u(x)*** and denote it by the same letter for sake of simplicity:

$$u(x,t) = u(x)e^{i\omega t}.$$

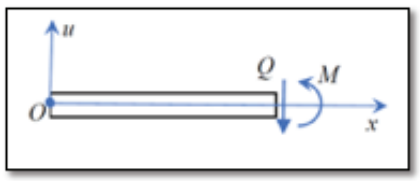

Figure 7. Beam model. Coordinate system and sign convention.

For harmonic vibration of a uniform beam in absence of external forces p, equation (11) reduces to

$$\frac{d^4 u(x)}{dx^4} - \kappa^4 u(x) = 0, \tag{14}$$

where

$$\kappa^4 = \frac{\rho A}{EI}\omega^2. \tag{15}$$

Taking the problem step by step, consider first the natural vibration of the free-free (unsupported) beam as if isolators and external excitation were absent. In this case, both shear forces and moments at both ends of the beam are zeroes; according to (12), (13), the boundary conditions for equation (14) are

$$u''(0) = 0;\ u''(L) = 0, \tag{16}$$

$$u'''(0) = 0;\ u'''(L) = 0. \tag{17}$$

This case is considered in many textbooks and handbooks on structural vibration. The following set of special functions, called Krylov functions, greatly simplifies dynamical calculations for beams:

$$S(x) = \tfrac{1}{2}(\cosh x + \cos x);\ T(x) = \tfrac{1}{2}(\sinh x + \sin x);\ U(x) = \tfrac{1}{2}(\cosh x - \cos x);\ V(x) = \tfrac{1}{2}(\sinh x - \sin x). \tag{18}$$

The general solution of the equation (14) in terms of Krylov functions is

$$u(x) = C_1 S(\kappa x) + C_2 T(\kappa x) + C_3 U(\kappa x) + C_4 V(\kappa x). \tag{19}$$

A remarkable property of Krylov functions is the circular relationship of their derivatives:

$$\frac{d}{dx}S(\kappa x) = \kappa V(\kappa x);\ \frac{d}{dx}V(\kappa x) = \kappa U(\kappa x);\ \frac{d}{dx}U(\kappa x) = \kappa T(\kappa x);\ \frac{d}{dx}T(\kappa x) = \kappa S(\kappa x). \tag{20}$$

Note that

$$S(0) = 1;\ T(0) = 0;\ U(0) = 0;\ V(0) = 0.$$

Using these properties, boundary conditions (16), (17) at ***x*** = 0 reduce (19) to

$$u(x) = C_1 S(\kappa x) + C_2 T(\kappa x).$$

Boundary conditions (16), (17) at ***x*** = L give, using (20), the system of two linear equations for C_1, C_2:

$$C_1 U(\kappa L) + C_2 V(\kappa L) = 0,$$
$$C_1 T(\kappa L) + C_2 U(\kappa L) = 0.$$

Solution exists if the determinant of this system equals zero, that is, the frequency satisfies the following characteristic equation for the non-dimensional frequency parameter $\beta = \kappa L$:

$$\det(\beta) = U^2(\beta) - T(\beta)V(\beta) = 0, \quad (20)$$

or, equivalently,

$$\cosh\beta \cos\beta - 1 = 0$$

The solutions, besides the trivial solution $\beta = 0$, are: $\beta_1 \approx 4.730$, $\beta_2 \approx 7.853$; $\beta_3 \approx 10.996$; subsequent roots closely follow $\beta_n = (2n+1)\pi/2$.

The non-dimensional parameter β defines the frequency. Let us assume the first natural frequency of flexural vibration of the platform $f_1 = 200$ Hz, which is a typical value for laboratory size optical tables. According to formula (15),

$$f_1 = \frac{1}{2\pi}\frac{\beta_1^2}{L^2}\sqrt{\frac{EI}{\rho A}},$$

where $\rho A = m/L$. Therefore, the bending stiffness of the beam must assume the value $EI = mL^3(2\pi f_1)^2/\beta_1^4$. The characteristic equation is illustrated by the thin blue line in Fig. 8. The first three natural frequencies of flexural vibration are found at 200 Hz, 551 Hz and 1081 Hz.

Now consider the full model of the elastic beam supported by springs. The modal shape of the beam satisfies equation (19) and boundary conditions (16) for zero moments. Pneumatic supports at both ends add frequency-dependent boundary conditions connecting transversal force with deflection. According to Eqs. (12), (13) and sign convention of Fig. 7, these boundary conditions take the following form:

$$EIu'''(0) = -K(\omega)u(0);\ EIu'''(L) = K(\omega)u(L), \quad (21)$$

where EI is the bending stiffness and $K(\omega)$ is the stiffness of the isolator (4). Applying boundary conditions at $x = 0$ to expression (19) leads to

$$C_3 = 0,\ C_4 = -\frac{K(\omega)}{\kappa^3 EI}C_1,$$

so that

$$u(x) = C_1\left(S(\kappa x) - \frac{K(\omega)}{\kappa^3 EI}V(\kappa x)\right) + C_2 T(\kappa x). \quad (22)$$

Boundary conditions at $x = L$ lead to the system of two linear equations for C_1, C_2:

$$C_1\left(U(\beta) - \frac{k_r(\omega)}{\beta^3}T(\beta)\right) + C_2 V(\beta) = 0,$$
$$C_1\left[T(\beta) - \frac{2k_r(\omega)}{\beta^3}S(\beta) + \left(\frac{k_r(\omega)}{\beta^3}\right)^2 V(\beta)\right] + C_2\left(U(\beta) - \frac{k_r(\omega)}{\beta^3}T(\beta)\right) = 0. \quad (23)$$

Here $\beta = \kappa L$ is assumed to be expressed as function of frequency ω, and $k_r(\omega)$ is a non-dimensional parameter characterizing the stiffness of isolator relative to the stiffness of the beam:

$$k_r(\omega) = \frac{K(\omega)L^3}{EI}. \quad (24)$$

In our case, $k_r(\omega) << 1$. In particular, since $k = m(2\pi f_0)^2/2$, and $EI = mL^3(2\pi f_1)^2/\beta_1^4$, we have $k_r(0) = (f_0/f_1)^2\beta_1^4/2 = (1\text{Hz}/200\text{Hz})^2 \cdot 4.730^4/2 \approx 6.257 \cdot 10^{-3}$.

The characteristic equation is

$$\det(\omega) = \left(U(\beta) - \frac{k_r(\omega)}{\beta^3}T(\beta)\right)^2 - \left[T(\beta) - \frac{2k_r(\omega)}{\beta^3}S(\beta) + \left(\frac{k_r(\omega)}{\beta^3}\right)^2 V(\beta)\right]V(\beta) = 0. \quad (25)$$

Here, again, β is substituted as function of frequency ω. The solutions are almost identical (within 0.01 Hz in terms of frequency) with that of (20), but two additional complex roots (damped frequencies) appear, practically coincident with the natural frequencies of the softly supported beam as a rigid body. The characteristic equation (22) is illustrated by the thick red line in Fig. 8.

To find the corresponding vibration modes, each solution of the characteristic equation is substituted into the system (23) for C_1, C_2 (or, rather, for the ratio C_1/C_2) and the resulting coefficients used in the equation (22). The

modes are defined up to a constant multiplier. The first two modes are vertical and rocking "rigid body" motions; the rest represent the flexural modes of the beam (Fig. 9).

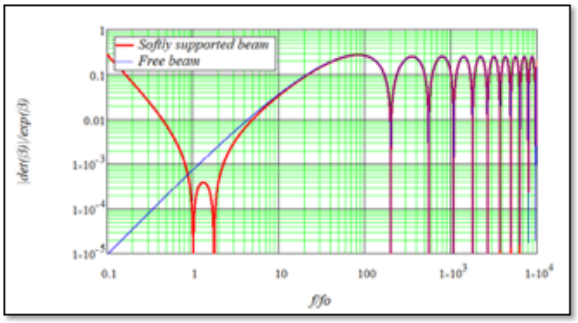

Figure 8. Graphical solution of the characteristic equation. Thin line – free-free beam, thick line – beam supported by soft pneumatic isolators. For a simpler graph, the real part of complex stiffness (devoid of damping) was used in generating this plot, to avoid graphing over a complex plane.

An important conclusion from this analysis is that as long as the ratio of "flexural" natural frequency to isolation frequency is as high as in this example, flexural deformation of the platform does not affect the isolation "bouncing" modes, and isolation does not affect the flexural vibrations of the platform. This large frequency span between the isolation (rigid-body) modes and flexural modes is a telltale sign of good vibration isolation design. It creates a large frequency range of vibration isolation unaffected by structural resonances.

For further insight into the dynamic properties of isolated platforms let us look at the forced vibration of our model under kinematic (Fig. 1(a)) and force (Fig. 1(b)) excitations.

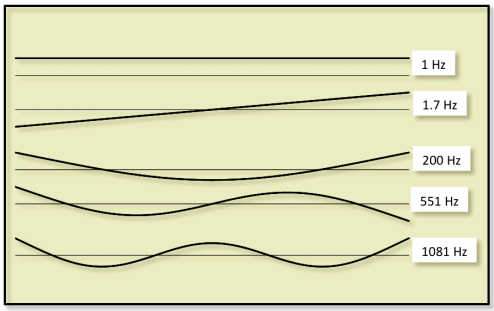

Figure 9. Rigid and flexural modes of the beam on soft isolators, drawn with the same amplitude.

In case of kinematic excitation of the foundation with the amplitude u_0, the boundary conditions are given by (16) and the following relationships between the displacements and transversal forces:

$$EIu'''(0) = -K(\omega)(u(0)-u_0);\ EIu'''(L) = K(\omega)(u(L)-u_0) \quad (26)$$

The general solution is, again, given by Eq. (19); boundary conditions at $x = 0$ lead to

$$C_3 = 0,\ C_4 = -\frac{k_r(\omega)}{\beta^3}(C_1 - u_0),$$

so that

$$u(x) = C_1 S(\kappa x) + C_2 T(\kappa x) - \frac{k_r(\omega)}{\beta^3}(C_1 - u_0)V(\kappa x). \quad (27)$$

Boundary conditions at $x = L$ lead to the system of two non-homogeneous linear equations for C_1, C_2:

$$C_1\left(U(\beta) - \frac{k_r(\omega)}{\beta^3}T(\beta)\right) + C_2 V(\beta) = -\frac{k_r(\omega)}{\beta^3}T(\beta)u_0,$$
$$C_1\left[T(\beta) - \frac{2k_r(\omega)}{\beta^3}S(\beta) + \left(\frac{k_r(\omega)}{\beta^3}\right)^2 V(\beta)\right] + C_2\left(U(\beta) - \frac{k_r(\omega)}{\beta^3}T(\beta)\right) = \left(-S(\beta) - 1 + \frac{k_r(\omega)}{\beta^3}V(\beta)\right)\frac{k_r(\omega)}{\beta^3}u_0, \quad (28)$$

where $\beta = \kappa L$ is assumed to be expressed as function of frequency ω. Resolving (28) for C_1, C_2, and substitution into (27) leads to an explicit formula for vibration transmissibility, $u(x)/u(0)$, at any point of the beam. To avoid infinite amplitudes at flexural resonances, damping with a loss factor $\eta = 0.01$ is introduced into the structure by substituting complex value $EI(1+i\eta)$ in place of EI.

The results are plotted in Fig. 10 along with the corresponding rigid-body solution shown by the thin lines. The graphs show that under the kinematic excitation the transmissibility, u/u_0, rolls off the same way as for a rigid body (single degree of freedom) at frequencies up to the vicinity of the first resonance frequency of flexural vibrations. At that frequency, large deviations from the rigid-body behavior occur. Due to the symmetric nature of the excitation, only symmetric vibration modes (see Fig. 9) are excited.

The analytical solution allows for a more detailed analysis providing insight into practically important questions about the relative displacement of points of the isolated platform and misalignment of parts of the platform (Fig. 11). These factors define the image movement and line-of-sight jitter that may affect the optical performance of an application residing on the vibration-isolated platform.

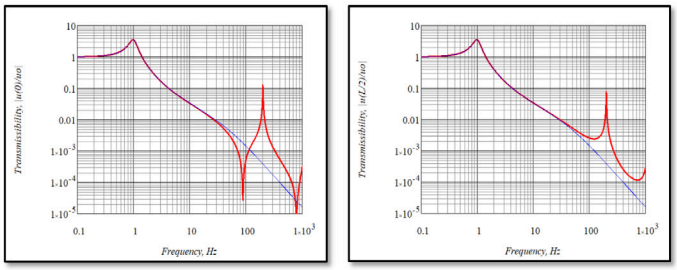

(a) (b)

Figure 10. Transmissibilities of the pneumatically isolated beam to the edge of the beam (a) and to the center of the beam (b). Thick line – full model, thin line – rigid beam. Only symmetric modes are excited by symmetric kinematic excitation, Fig. 1(a).

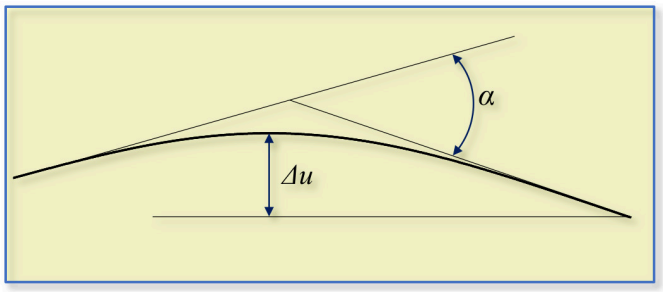

Figure 11. Maximum relative displacement (Δu) and misalignment (a) of the central axis of a beam.

Figure 12 shows the maximum relative displacement, Δu, of two points of the beam, and maximum misalignment (the maximum difference between slopes, $\alpha = u'(x)$, at two points of the beam) in case of kinematic excitation from the floor with the amplitude u_0 (Fig. 1(a)). The results reveal that even in the rigid-body zone small quasi-static deformations occur that do not roll-off with frequency. These deformations are caused by inertia forces generated by slow oscillations. At the flexural resonance, the misalignment increases sharply; relative displacement reaches almost twice the absolute resonance response.

In case of force excitation, Fig. 1(b), the boundary conditions that reflect the relationship between the displacements and transversal forces are

$$EIu'''(0) = -K(\omega)u(0) + F;\ \ EIu'''(L) = K(\omega)u(L). \qquad (29)$$

Further calculations of the complex amplitude $u(x)$ are completely analogous to the case of kinematic excitation. These calculations lead to the dynamic compliance at the excitation point and transfer functions to other points of the beam plotted in Fig. 13. The "rigid body line" is a straight line with a slope $1/f^2$ (40 dB per decade) corresponding to Newton's Second Law (acceleration proportional to force). The graph shows large deviations from the rigid-body response at the first and second bending modes of the beam (Fig. 9).

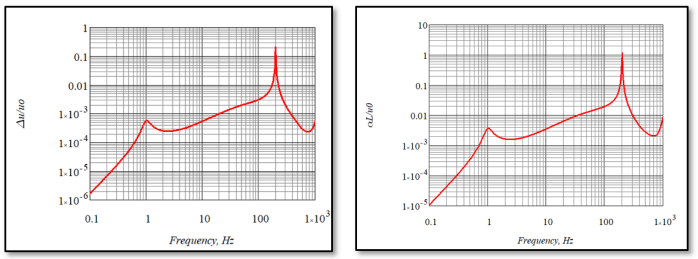

(a) (b)

Figure 12. (a) Maximum relative displacement between points of the pneumatically isolated beam, Δu, and (b) maximum misalignment between areas of the beam, a, caused by kinematic excitation u_0 from the foundation.

Calculating the relative displacement of points of the beam under the force excitation due to flexural vibrations requires subtraction of the rigid-body motion; misalignment can be obtained by direct differentiation of the deflection. The results, shown in Fig. 14, show that even in the rigid-body zone small quasi-static deformations occur that do not roll-off with frequency. These deformations are caused by inertia forces generated by slow oscillations. At the flexural resonance the misalignment increases; relative displacement reaches almost twice the absolute resonance response at the first bending mode (200 Hz) and about twice the absolute resonance response at the second bending mode (551 Hz).

These calculations reveal that even in the “rigid body” range, away from flexural resonances, the isolated platform does not behave as absolutely rigid. Small quasi-static deflections are noticed in the frequency range of rigid-body behavior of the beam (up to about 150 Hz). Quasi-static bending exists even in the single Hz and even sub-Hz frequency ranges, amplified by the isolator resonance. This is deformation caused by slowly changing inertia forces. These quasi-static deformations are orders of magnitude smaller than absolute displacements away from the flexural resonances and generally not discernible by standard dynamic compliance test in the “rigid body” frequency range. Most applications are not sensitive to these small deformations. However, in some high-precision applications quasi-static bending of isolated platform or payload structures such as bridges that may be substantial enough to affect the optical performance. This phenomenon gives motivation for developing more advanced active vibration isolation systems.

As expected, large deviations from rigid-body behavior around the resonance frequencies are accompanied by large misalignments and relative flexural displacements of points of the beam. Peak relative displacement at the flexural resonance is about twice the absolute displacement.

Note that it is common practice[5] to plot the transmissibility in a low-frequency range encompassing isolation resonances and part of the rigid-body frequency range, and plot the dynamic compliance at higher frequencies, encompassing the rigid-body range and resonance frequencies. This is related to the limitations of generally adopted experimental techniques. The analytical model considered in this Technical Note is free of these limitations and allows us to review simultaneously all aspects of the dynamic behavior of the isolated platform in a wide frequency range.

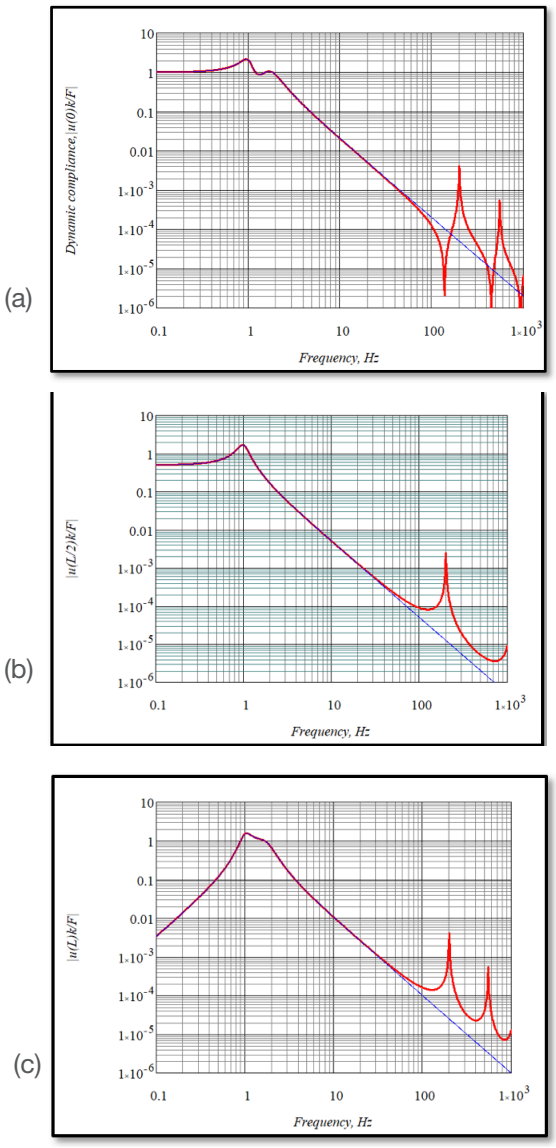

Figure 13. Dynamic compliance at the end of the beam (a), transfer functions from the force at one end of the beam to the displacement at the middle of the beam (b) and to the other end of the beam (c). Thick line – beam supported by pneumatic isolators, thin line - rigid beam of equivalent mass. All functions are referred to the static compliance, $1/k$.

(5) https://www.newport.com/n/compliance-and-transmissibility-curves

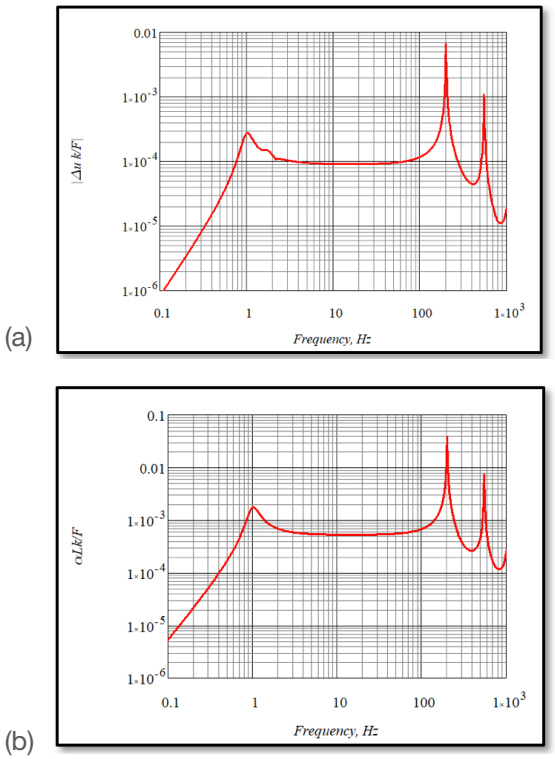

Figure 14. (a) Maximum relative flexural displacement between points of the pneumatically isolated beam, Δu; (b) maximum misalignment between two areas of the beam, α, caused by force excitation, per unit force. All functions are referred to the static compliance, $1/k$.

Although this model captures the main physical properties of isolated platforms, there are substantial differences from real optical tables. The most significant difference is that a table, being a plate-like structure able to deform in three dimensions, has a denser spectrum of resonance frequencies. Several resonances can be usually observed in the 100 Hz – 1000 Hz range. That makes the goal of expanding the "rigid-body" frequency range by the platform design even more important.

C. Role of Mass and Bending Stiffness

The analytical model allows for easy investigation into the influence of design parameters of the platform, namely, structural and non-structural mass and bending stiffness, on the dynamic behavior. This information helps in choosing a proper isolated platform for sensitive optical applications.

To analyze the influence of non-structural mass, suppose we double the mass of the beam (and, accordingly, the moment of inertia) without increasing the bending stiffness. The stiffness of the pneumatic isolators adjusts to keep the first isolation frequency the same at 1 Hz. Figure 15 shows the resulting vibration transmissibility, dynamic compliance, and relative motion for kinematic and force excitation compared to the base case. Misalignment generally mirrors the relative displacement, so misalignment graphs are not shown here. The comparison shows that, as a result of adding non-structural mass, the frequency range of the rigid-body behavior is reduced; the flexural resonance frequency becomes lower; the peak resonance response is increased; more resonance frequencies enter the depicted frequency range. Quasi-static relative motion increases with increased mass under floor excitation and stays the same under force excitation.

The behavior of the relative motion has a simple physical interpretation. The maximum relative motion of points in a structure is roughly proportional to the motion relative to the center of mass (CG), usually by a factor of 2. To describe the motion of the structure in the coordinate system tied to the CG, we must apply inertia forces to the structure. Inertia force on any material particle equals its mass times acceleration of the coordinate system. Therefore, elastic deflections, defined by the inertia forces, are proportional to the mass time acceleration of the CG. Acceleration equals displacement times $(2\pi f)^2$ in the frequency domain. The motion of the CG is the same as rigid-body motion. Under the force excitation, rigid-body displacement rolls-off like $1/f^2$, that is why the graphs of relative motion and misalignment look flat in the rigid-body frequency range. If the mass is doubled, but the rigid-body acceleration is reduced two times, the inertia force, and therefore relative motion and misalignment, stay the same. Under kinematic excitation from the foundation, the rigid-body transmissibility stays

the same, so doubling the mass (and therefore the inertia forces) leads to doubling of the relative displacement and misalignment.

In the same manner, we can research the effect of increasing bending stiffness, as well as simultaneous increase of mass and stiffness (adding structural mass). Figures 15 – 18 illustrate the transmissibilities, dynamic compliances and relative displacements under kinematic and force excitation for different scenarios of increasing stiffness or simultaneous increase of mass and stiffness. (Misalignments behave generally the same way as relative displacements, so no additional graphs are given here). The graphs are accompanied by lists of positive and negative effects of the change in parameters on various aspects of the dynamics of the platform. Positive effects are shown in green, negative in red, neutral – in blue letters.

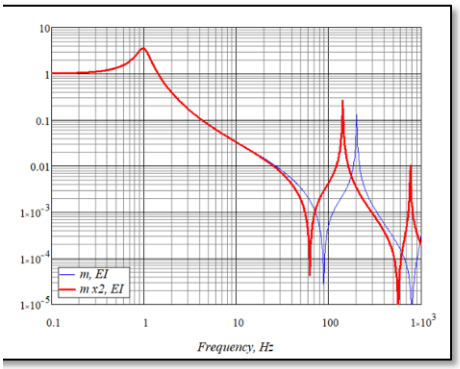

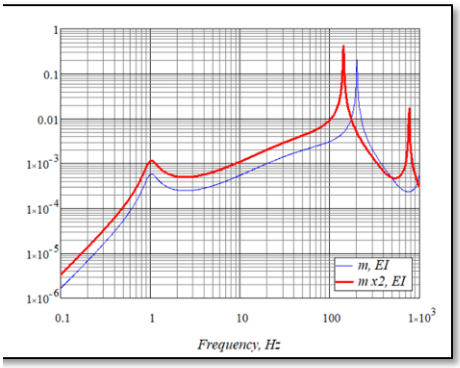

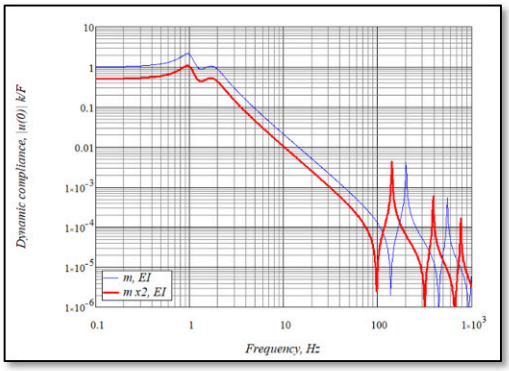

(c)

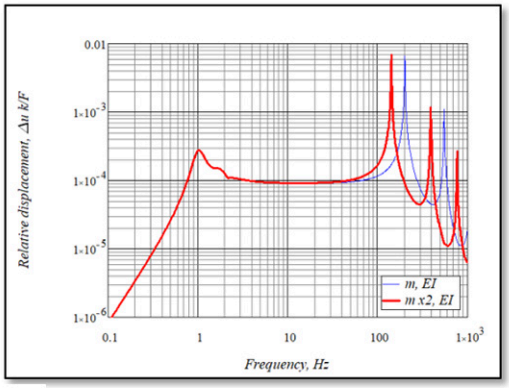

(d)

Figure 15. Effect of non-structural mass on (a) Transmissibility (b) Maximum relative displacement per unit floor excitation; (c) Dynamic compliance; (d) Maximum relative displacement per unit force. The last two functions are referred to the static compliance in the base case, 1/k.

Effect of increased non-structural mass:

- The frequency of rigid behavior **contracts**
- More resonances may appear in a given frequency range
- Quasi-static bending due to floor excitation **increases**
- Amplitudes of flexural resonances due to floor excitation increase
- "Rigid body line" of compliance **shifts down**
- Quasi-static bending due to force excitation stays the same
- Amplitudes of flexural resonances due to force excitation stay the same

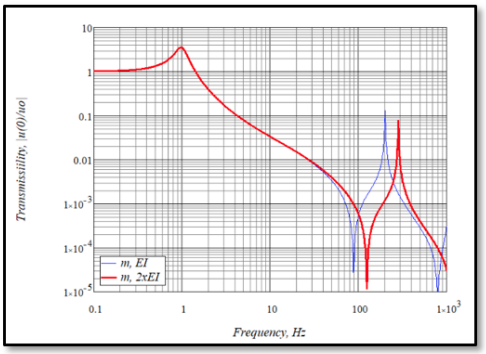

(a)

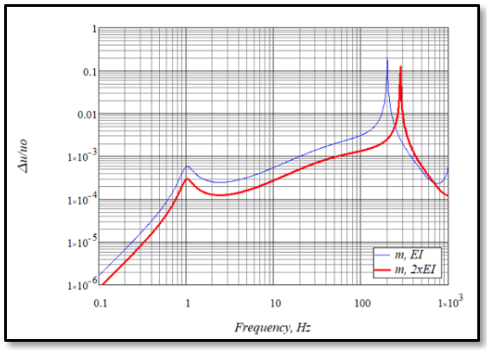

(b)

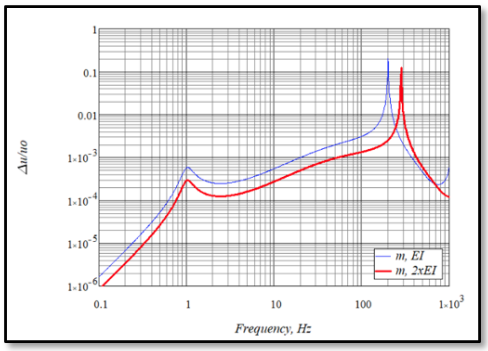

(b)

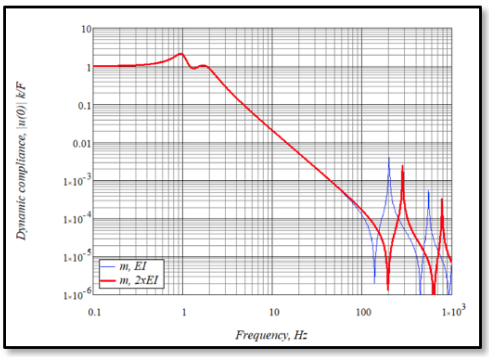

(c)

Figure 16 (left). Effect of increased bending stiffness on (a) Transmissibility (b) Maximum relative displacement per unit floor excitation; (c) Dynamic compliance; (d) Maximum relative displacement per unit force. The last two functions are referred to the static compliance in the base case, $1/k$.

Effect of increased bending stiffness:

- The frequency range of rigid behavior **expands**
- Quasi-static bending due to floor excitation **decreases**
- Amplitudes of flexural resonances due to floor excitation decrease
- "Rigid body line" of compliance stays the same
- Quasi-static bending due to force excitation **decreases**
- Amplitudes of flexural resonances due to force excitation **decrease**

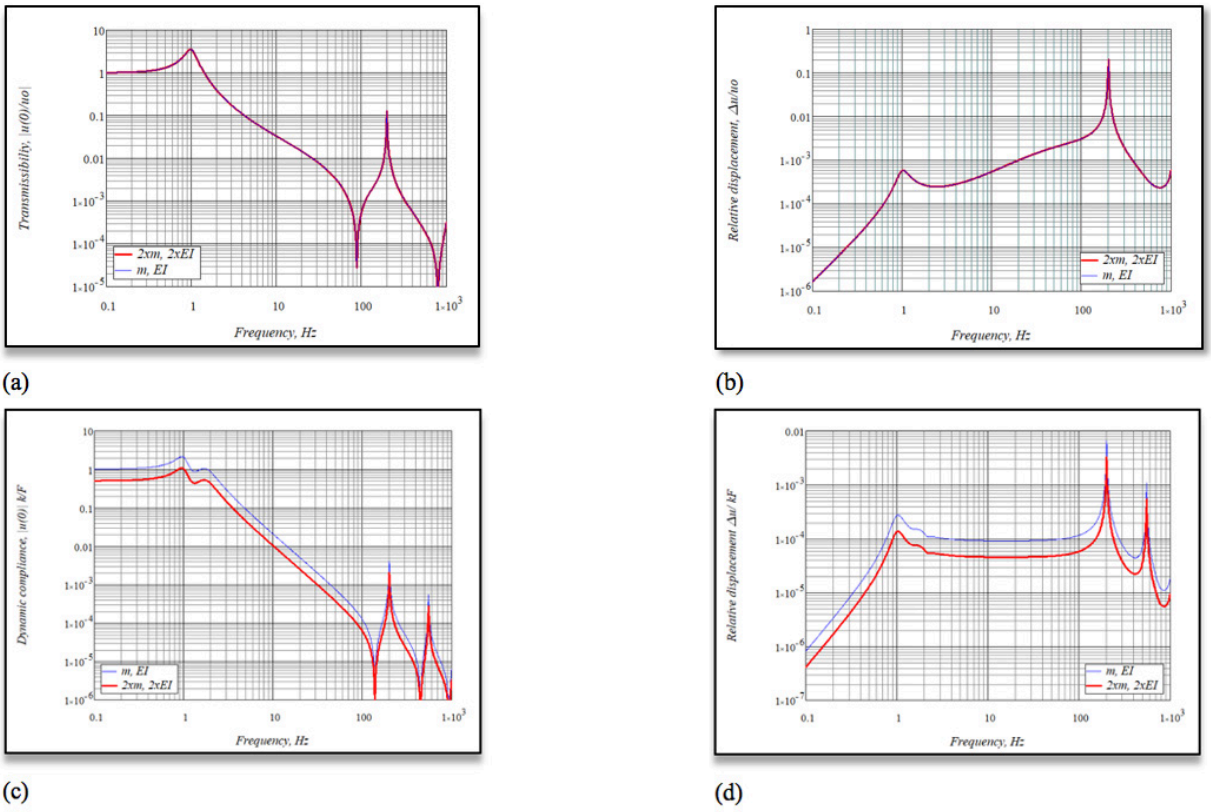

Figure 17. Effect of structural mass on (a) Transmissibility (b) Maximum relative displacement per unit floor excitation; (c) Dynamic compliance; (d) Maximum relative displacement per unit force. The last two functions are referred to the static compliance in the base case, $1/k$.

Effect of structural mass (mass and bending stiffness increase in the same proportion):

- The frequency range of rigid behavior stays the same
- Quasi-static bending due to floor excitation stays the same
- Amplitudes of flexural resonances due to floor excitation stay the same
- "Rigid body line" of compliance shifts down
- Quasi-static bending due to force excitation decreases
- Amplitudes of flexural resonances due to force excitation decrease

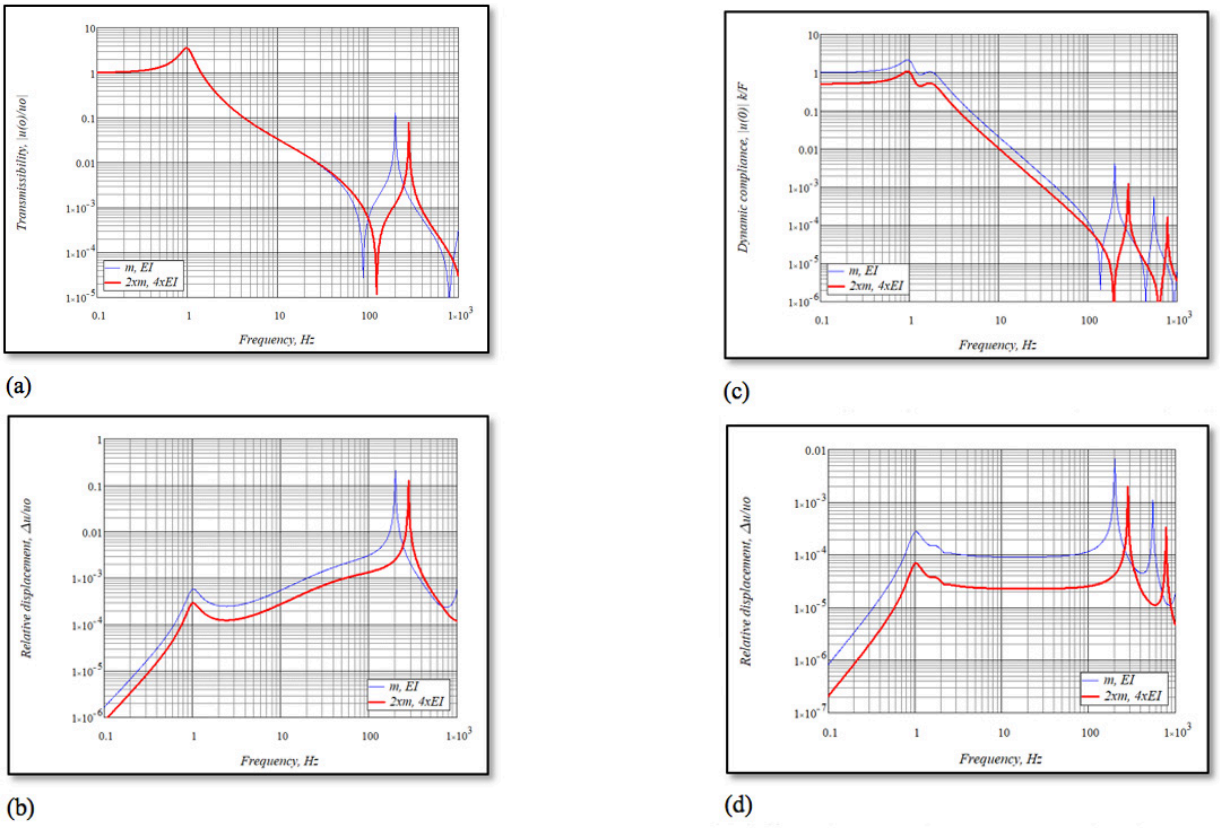

Figure 18. Effect of "super-structural" mass (bending stiffness increases in higher proportion than mass) on (a) Transmissibility (b) Maximum relative displacement per unit floor excitation; (c) Dynamic compliance; (d) Maximum relative displacement per unit force. The last two functions are referred to the static compliance in the base case, $1/k$.

Effect of "super-structural" mass (bending stiffness increases in higher proportion than mass):

- The frequency range of rigid behavior **expands**
- Quasi-static bending due to floor excitation **decreases**
- Amplitudes of flexural resonances due to floor excitation **decreases**
- "Rigid body line" of compliance **shifts down**
- Quasi-static bending due to force excitation **decreases**
- Amplitudes of flexural resonances due to force excitation **decrease**

Note that if bending stiffness and mass increase in the same proportion (2 times), transmissibility and relative motion under kinematic excitation from the floor stay the same (hence no new graph appears this case); however, the dynamic response under force excitation does change (see Fig. 17). Increasing bending stiffness invariably leads to improvement in dynamic qualities; the best results are obtained when stiffness increases simultaneously with mass but in higher proportion. Figure 18 shows the result of increasing mass 2 times and bending stiffness 4 times. In application to real-life optical tables, the latter case describes the effect of increasing the thickness of the table. The effect of thickness on the table performance is illustrated by Fig. 19 that depicts experimental dynamic compliances of 305 mm thick table and 203 mm thick table of the same dimensions.

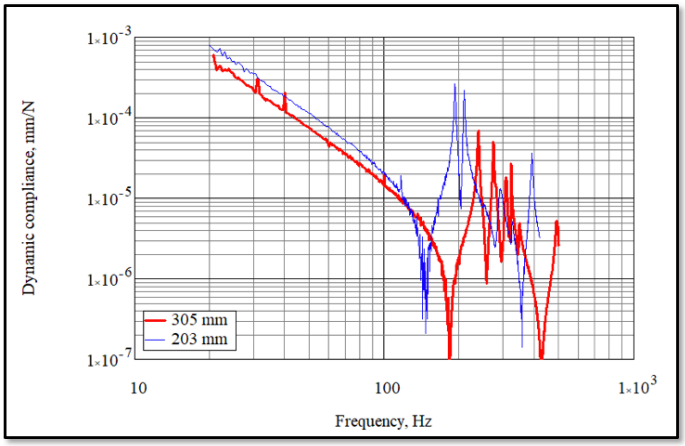

Figure 19. Experimental corner dynamic compliances of optical tables 1.22 m x 2.44 m of different thicknesses. The tables did not use any additional means of damping except structural damping.

An important conclusion from this model example is that the increase of the mass of the pneumatically isolated platform by itself gives no advantage, except in applications when the absolute motion of the platform is important (for example, if a laser beam must be referenced to a target outside of the table). Most high-precision applications are confined to one table.

In this case, it is the relative motion of parts of the table and misalignment of portions of the surface that matters. Increasing mass does not change the relative motion and misalignment under on-board or acoustical impacts; moreover, the relative motion and misalignment under kinematic excitation from the floor will increase proportionally to the mass. Since pneumatic isolators adjust to the increased load to keep the isolation frequency the same, the isolation efficiency does not change. On the other hand, the frequency interval of rigid-body behavior shrinks with the increase of mass, and resonance amplitudes become higher.

Increasing mass can be beneficial only if accompanied by at least proportional increase in the bending stiffness of the platform. This observation adds clarity to the often-discussed question concerning the design of honeycomb optical tables: does it pay to use denser honeycomb cores? Denser core increases the mass of the table; it also increases the shear modulus of the core. However, the stiffness of the table is defined mostly by the facesheets that work in compression – tension when the table bends, with a relatively small contribution of the shear modulus of the core. So, the increase in total bending stiffness by a denser core will be less than proportional to the increase of mass. A heavier core leads to net deterioration of the dynamic quality of the table.

To improve the dynamic properties of the table, we need to increase the bending stiffness more than we increase the mass. As mentioned above, one way to achieve it is to increase the thickness of the table (see Fig. 19).

A radical way to improve the dynamic properties of the isolated platform is to reduce or eliminate the resonance peaks through damping, that is, dissipation of mechanical energy. Dynamic vibration absorbers, or tuned mechanical dampers (TMD), are known to be the most effective devices for this purpose. TMD is a damped oscillator tuned to a certain frequency close to the resonance frequency that we intend to suppress.

D. Effect of Tuned Mass Dampers

The beam model of an isolated platform allows for simulation of the effect of tuned mass dampers. They can be modeled as damped oscillators attached to the ends of the beam (Fig. 20).

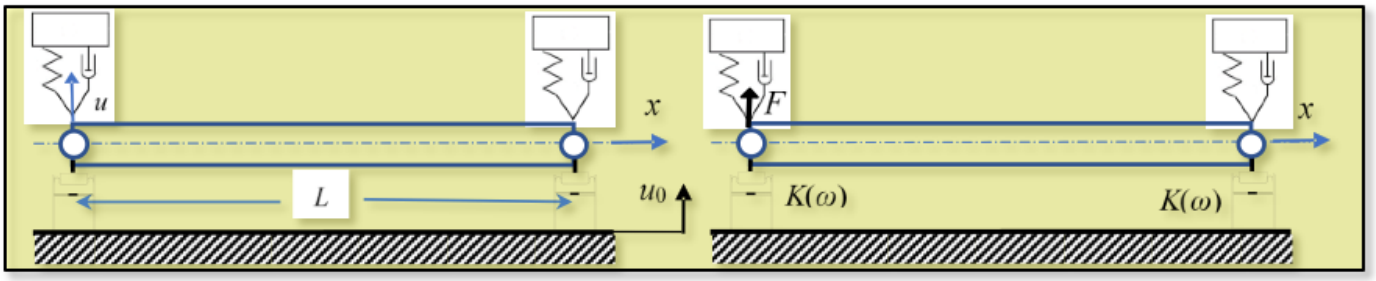

(a) (b)

Figure 20. Model of the isolated platform with dynamic vibration absorbers (TMD).

To find the vibration amplitudes, we'll need the expression for dynamic stiffness, that is, the ratio of complex amplitudes of force acting on the oscillator at the attachment point to the displacement at this point:

$$K_a(\omega) = \frac{-m_a\omega^2}{1-\dfrac{\omega^2}{\omega_a^2(1+i\eta_a)}},$$

where m_a is the mass of the damper, ω_a is the partial circular frequency (tuning frequency) of the damper, and η_a is the loss factor. The frequency-dependent boundary conditions for the beam equation (14) are given by (16) and

$$EIu'''(0) = -K(\omega)(u(0)-u_0) - K_a(\omega)u_0;\ EIu'''(L) = K(\omega)(u(L)-u_0) + K_a(\omega)u_0 \tag{30}$$

in case of kinematic excitation of the foundation with the amplitude u_0, Fig. 20(a), or

$$EIu'''(0) = -\left[K(\omega)+K_a(\omega)\right]u(0) + F;\ EIu'''(L) = \left[K(\omega)+K_a(\omega)\right]u(L). \tag{31}$$

in case of force excitation at $x = 0$, Fig. 20(b). Further calculations of the complex amplitudes $u(x)$ are straightforward, following the procedure outlined above.

The theoretical basis for optimization of dynamic vibration absorbers is well developed. A summary with application to optical tables can be found in the article[6]. Parameters of the dynamic absorbers are determined based on their mass ratios, following the optimization formulas

$$\frac{\omega_a}{\omega_k} = \frac{1}{1+\mu_k},\quad \eta_a = \sqrt{\frac{(3+2\mu_k)\mu_k}{2+\mu_k}}. \tag{32}$$

Here, $\omega_k = 2\pi f_k$ is the targeted resonance circular frequency: $u_k = m_k/m$, where m_k is the effective modal mass. Assume the masses of each absorber m_a = 0.025m (2.5% of the mass of the platform). Direct calculation (omitted here) gives effective modal masses m_k = 0.25m, so that u_k = 0.1. Therefore, the damper tuned to the first flexural resonance at 200 Hz should have, according to (32), partial resonance frequency f_a = 182 Hz; the damper tuned to the second flexural resonance at 551 Hz, partial resonance frequency f_a = 501 Hz. The optimal loss factor is, according to (32), n_a = 0.39. Figures 21 and 22 illustrate transmissibilities and dynamic compliances for two cases: first, both

(6) V.M. Ryaboy, Practical aspects of design, tuning and application of dynamic vibration absorbers, Proceedings of Meetings on Acoustics, Vol. 26, 065006 (2016); http://doi.org/10.1121/2.0000231.

dampers are tuned to the first resonance; second, one damper (at $x = 0$) is tuned to the first resonance and the second damper (at $x = L$) – to the second resonance. Again, the stiffness of pneumatic isolators adjusts to slightly higher load (with the added weight of dampers) to keep the "bouncing" frequency constant. In case when both dampers are tuned to the first resonance peak, it is reduced almost 20 times (Fig. 21), however, the second peak stays almost the same. When dampers are tuned to separate peaks (Fig. 22), both resonances are suppressed, but to a lesser extent. Relative motion and misalignment in the resonance zone are reduced accordingly.

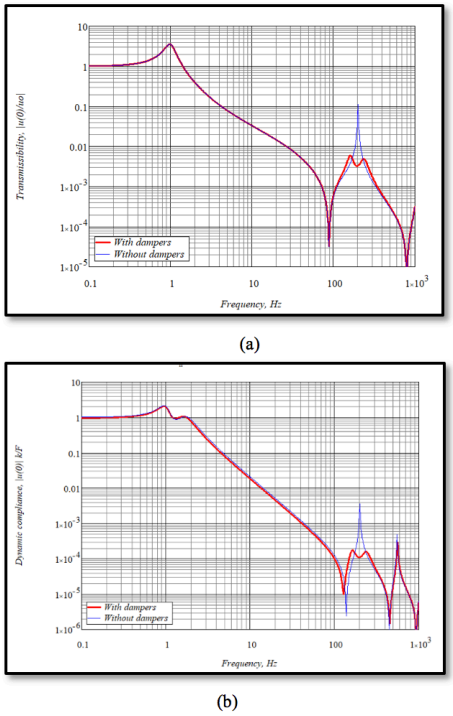

Figure 21. Transmissibility (a) and dynamic compliance (b) of the model of the isolated platform with both dampers tuned to suppress the first flexural resonance.

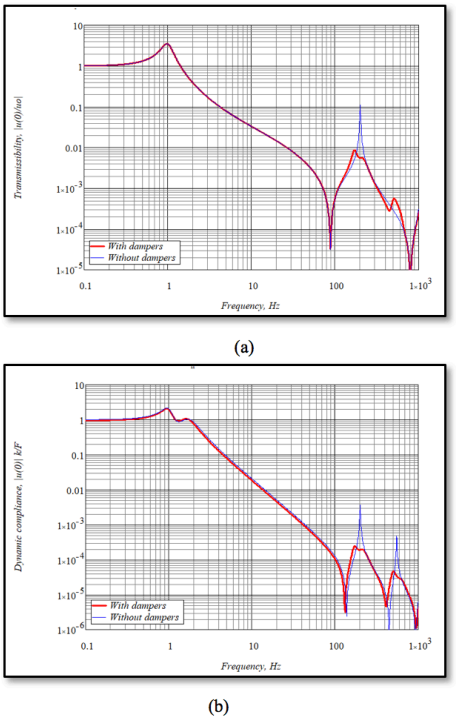

Figure 22. Transmissibility (a) and dynamic compliance (b) of the model of the isolated platform with one damper tuned to suppress the first flexural resonance, another one – the second flexural resonance.

This model example shows that dynamic vibration absorbers (tuned mass dampers) can greatly reduce deviations from rigid-body behavior. Patented designs of these dampers are employed in the MKS RS series optical tables[6].

E. Take-home Conclusions

- Vibration isolation system consists of soft isolators and stiff platform
- The vibration modes comprise “rigid body” modes and flexural modes
- Isolators and overall mass and moments of inertia are responsible for “rigid body” (bouncing) modes
- State-of-the-art pneumatic isolators keep the “rigid body” natural frequencies approximately constant in a wide range of loads
- Bending stiffness and mass distribution of the platform are responsible for flexural modes
- Large deviations from rigid-body behavior can happen near flexural vibration natural frequencies
- Well-designed vibration isolation system has low (down to 1 Hz) “rigid body” natural frequencies and high flexural vibration natural frequencies
- The frequency range of maximum isolation effect is the “rigid body” interval between the bouncing and flexural natural frequencies
- Even in the “rigid body” zone, small quasi-static bending exists due to inertia forces
- To improve the quality of vibration isolation, bending stiffness of the isolated platform must be increased in higher proportion than mass
- Flexural resonances can be effectively suppressed by tuned mass dampers.

mks | Newport™

www.newport.com

DS-032201 (04/22)
©2022 MKS Instruments, Inc.
Specifications are subject to change without notice.

MKS products provided subject to the US Export Regulations. Diversion or transfer contrary to US law is prohibited. mksinst™ is a trademark of MKS Instruments, Inc., Andover, MA.